Pis'ma v ZhETF, vol. 95, iss. 12, pp. 738 – 743 © 2012 June 25

Self-assembly of charged CdTe nanoparticles

D. N. Voylov[+*1)], *L. M. Nikolenko*, *D. Yu. Nikolenko*[°], *N. A. Voylova*, *E. M. Olsen*[×], *V. F. Razumov*

[+]*Joint Analytical Center, Scientific Center in Chernogolovka RAS, 142432 Chernogolovka, Russia*

[*]*Laboratory of Physical and Chemical Investigations, Institute of Problems of Chemical Physics RAS, 142432 Chernogolovka, Russia*

[°]*Laboratory of Photonics of Nanosized Structures, Institute of Problems of Chemical Physics RAS, 142432 Chernogolovka, Russia*

[×]*Department of Physics and Astronomy, University of Tennessee, Knoxville, 37996 Tennessee USA*

Submitted 20 March 2012
Resubmitted 25 April 2012

Here we show a method of the organization of charged CdTe nanoparticles which allows the generation of a self-assembled monolayer of above 10.000 μm^2 in a time of about 90 s. The analysis of adsorption kinetics of particles on a surface shows that it is well described by the Langmuir isotherm. We have found that thermal and electrical conductivity of a substrate play an important role. Nevertheless, deficiency of a substrate doesn't affect the adsorption kinetic. The structure of a formed monolayer essentially depends on pH and as a consequence on the particles' charge. This method can be effective for the production of a CdTe nanoparticle's monolayer with well controlled area and a degree of filling on a surface.

Introduction. The self-assembly of nanoparticles is connected to prospects of nanostructures in sensors [1], nanoelectronics [2, 3], photonics devices [4] and in fundamental research [5]. In the last decade there were many experimental and theoretical works devoted to the study of mechanisms responsible for the self- organizing of particles at evaporation of a solution [6–14]. Now it is well-known that at evaporation the deposit structure depends on many factors: Reynolds and Weber numbers, heat capacity and thermal conductivity of the substrate [15] and as a result Marangoni forces [16], pH and volatility of the solution [17], charge of the particles and substrate [18], application of dc or ac electric, or magnetic [19] fields etc. Meanwhile, in photovoltaics applications, at creation of high-sensitivity sensors and other devices [20], the finding of modes of controllable self-organizing in one [21], two and three dimensional structures [22] is important. Here, we show a method of the organization of charged CdTe nanoparticles which allows for the generation of a monolayer above 10.000 μm^2 in about 90 s.

Chemicals. Te powder (30 mesh, 99.997%), tributylphosphine (TBP) (97%), oleic acid (OA) (90%), 1-octadecene (ODE) (tech. 90%) were purchased from Aldrich; CdO (99.99%) were purchased from Sigma Aldrich; MPA were purchased from Fluka. KOH (reagent grade) and methanol (reagent grade) were purchased from KhimMed.

Synthesis of CdTe Nanocrystals. The synthetic method were similar to the one reported previously [23]. A typical synthetic procedure was as follows. Te solution was prepared by dissolving 0.009 g (0.070 mmol) of Te powder in 0.0987 g of TBP and then diluted with ODE to 2 g under Ar flow. 0.0127 g (0.1 mmol) of CdO and 0.1257 g (0.44 mmol) of OA were loaded into a three-neck flask and heated to 260 °C under Ar flow to obtain a clear solution. Then the Te solution was quickly injected into the hot solution of Cd precursor. After injection the reaction mixture was allowed to cool to 100 °C for the growth of the CdTe nanocrystals. The reaction mixture was then cooled to room temperature using a water bath. The synthesis was carried out under Ar flow.

Preparation of water-soluble nanocrystals. The method described in the Ref. [24] was used to prepare negatively charged MPA capped water-soluble CdTe. 0.5 M methanolic solution of MPA-KOH (with 20 mol % excess of KOH) was added to solution of CdTe QDs in chloroform until the particles flocculated. After the flocculation, distilled water was added to form a two-phase system. Then the solution was left until all the QDs were transferred from chloroform phase into the water phase.

Experimental techniques and sample preparation. AFM and STM measurements were performed using Scanning Probe Nanolaboratory Integra Aura (NT-MDT, Russia). We used two types of tips: standard silicon tips with curvature radius about 10 nm and supersharp DLC tips with curvature radius about 1 nm (all NT-MDT, Russia). STM measurements were provided under low vacuum (about 50 mbar) using standard PtIr and W tips.

[1)] e-mail: voilov@icp.ac.ru

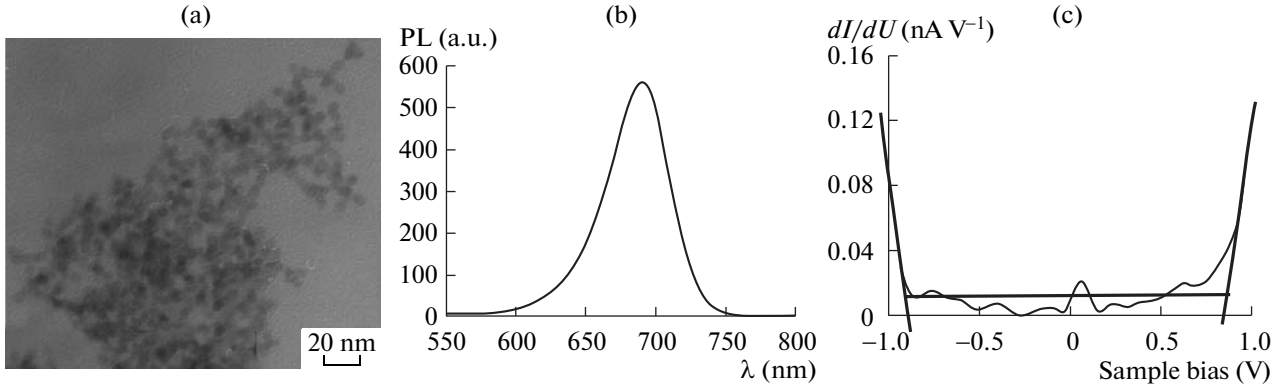

Fig. 1. Initial characterization of the nanoparticles. (a) – TEM data of the CdTe nanoparticles. (b) – Photoluminescence spectra of CdTe solution. (c) – STM measurement results of CdTe nanoparticles' monolayer on the HOPG surface. PtIr tip was used. This data was obtained by averaging of more than 25 measured curves. Estimated energy band gap $E_g = 1.78$ eV was in a perfect agreement with the value obtained by absorption spectra.

TEM measurements were carried out with JEM-2100 (JEOL, Japan) using Cu TEM grids covered by amorphous carbon.

We used LS 55 Fluorescence Spectrometer (Perkin Elmer, USA) to obtain luminescence spectra. Solutions were contained into the 10 mm quartz cells.

A drop of solution in a volume of $10\,\mu$l was drop casted by the dispenser on a substrate and was absorbed by filter paper (without touching of the surface) after certain time. For positive nanoparticle identification at deposition times the following operations were performed: a fresh flake of HOPG attached to the pyroceramic substrate with bi-adhesive tape, was placed on the scanner with a maximum scanning range of 100 microns. In the beginning, a number of measurements detected displacement of the substrate due to the reverse deformation of the bi-adhesive tape. As a result, the sample was left untouched for the day then was scanned again. This procedure was performed until the displacement was within acceptable bounds (not more than 20 nm/15 min).

In our studies, we used negatively charged nanoparticles of about 4.5–5 nm (Fig. 1), obtained by high-temperature colloidal synthesis and then hydrophilized by the method described in detail in the recent work [24]. Such particles are interesting because they retain their stability over a long period of time. We carried out comparative measurements on two solutions: one was stored in inert atmosphere for six months while the other was freshly prepared. During the measurements, we observed a small quantity (about 5%) of three-dimensional clusters being greatly larger than the size of the particles in the older solution. The results showed identical kinetics of self-organization on the substrate of the particles for both solutions, which means the clusters had no crucial effect on the kinetic of self-assembly.

Our experimental technique included low volatility of a solvent (a water solution of ammonia), small times of sedimentation and high thermal conductivity of a substrate.

We have found the optimal concentrations of particles in a solution ($6 \cdot 10^2$ to $6 \cdot 10^4\,\mu\mathrm{m}^{-3}$) to obtain a monolayer on the HOPG surface. During the experiment, we observed the following growth behavior of the particle monolayer as shown in the Fig. 2.

According to experimental data it is possible to conditionally allocate two stages – a primary attachment of particles (initial) and monolayer growth (a growth stage initiated by the first stage):

1) the initial stage of monolayer formation occurs for $\Delta t_1 \leq 10$ s. This stage is characterized by the single particle's adsorption and up to 20 nanoparticle's monolayers (Fig. 2a);

2) the growth stage occurs for $\Delta t^2 > 10$ s. After attaching particles to the surface the monolayer starts to grow. This should be followed by initiation and increase of the diffusion flow, directed to the surface. However, given the concentration we used, this flow does not play a decisive role in monolayer formation. For a rough estimation we will consider water-ammonia (80–20%) solution which has a slightly lower density than one used in our experiments. At the diffusion coefficient ($D \approx 62.4\,\mu\mathrm{m}^2 \cdot \mathrm{s}^{-1}$ at $\eta \approx 1.25$ mPa $\cdot$ s [25], $T = 293$ K) for these particles the mean-square displacement $\langle r^2 \rangle$ in one second will be about $11.2\,\mu$m. For 30 s at concentration $n_0 = 1.89 \cdot 10^3\,\mu\mathrm{m}^{-3}$, surfaces with an area of $1\,\mu\mathrm{m}^2$ will reach on average $\frac{1}{3} n_0 S \sqrt{2Dt} = 3.86 \cdot 10^4$ particles. This value is about 2.7 times greater than the number

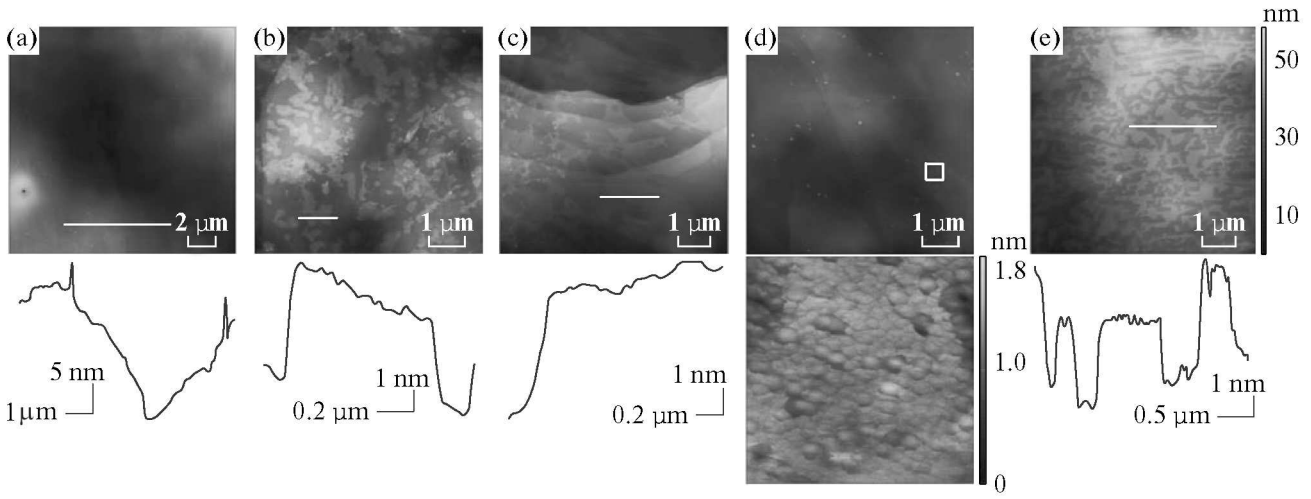

Fig. 2. AFM data of CdTe monolayers. The top figures are 2D AFM images obtained by tapping mode. The bottom figures are the cross-sections of the monolayers area shown on the top images by line. (a), (b), (c) and (d) are results related to deposition time of 10, 30, 60, and 90 s respectively for concentration of solution $C = 1.89 \cdot 10^3\ \mu\text{m}^{-3}$ (bottom image on (d) is the surface of the area shown in the top image with rectangle obtained with AFM using 1 nm curvature radius tip). (e) – Result of deposition of the nanoparticles during 60 s for maximal concentration $C = 6.033 \cdot 10^3\ \mu\text{m}^{-3}$

Concentration of solution, μm^{-3}	Deposition time, s	Average surface density of particles, $\langle\sigma\rangle \cdot 10^4\ \mu\text{m}^{-2}$ (We used the value of nanoparticle's area about $S_p = 2.376 \cdot 10^{-5}\ \mu\text{m}^2$)	Adsorption kinetic effective rate constant, k_c	$N_{\max}$ (maximum number of particles in a monolayer island in which could be inscribed a square area of $1\ \mu\text{m}^2$)
$6 \cdot 10^2$	30 ± 3	1.248	$3.3 \cdot 10^{-3}$	$1.31258 \cdot 10^5$
	60 ± 3	2.321		
	90 ± 3	3.342		
	105 ± 3	3.801		
$1.89 \cdot 10^3$	30 ± 3	1.410	$3.7 \cdot 10^{-3}$	$1.31258 \cdot 10^5$
	60 ± 3	2.596		
	90 ± 3	3.741		
$6 \cdot 10^4$	30 ± 3	1.695	$4.5 \cdot 10^{-3}$	$1.31258 \cdot 10^5$
	60 ± 3	3.116		
	70 ± 3	3.580		

of adsorbed nanoparticles (taking into account supposed packing density – 0.9069) for the same time on the same area (see Table).

Because the observable picture of the sedimentation process on the HOPG surface in many respects is similar to the monomolecular adsorption usually described by the Langmuir isotherm [26], we have applied a simplified model with the kinetic equation:

$$n(t) = N_{\max}(1 - e^{-k_c t}), \qquad (1)$$

where $N_{\max}$ is the maximum number of particles in a monolayer island in which a square area of $1\ \mu\text{m}^2$ could be inscribed and k_c is the effective adsorption rate constant. The description of experimental data by this function is shown in Fig. 3b. Analysis of the measured data allows us to conclude that the relation of the areas is $\frac{S_m}{S_0} \approx 3.44$, where S_0 is the visible part of the AFM images covered area by the nanoparticles on the HOPG surface and S_m is the real area of this monolayer. It means that when we observe the fully covered scanning area S_0, the real area S_m of the monolayer is bigger by a factor of 3.44. This fact can be easy understandable if we take into account the fractal properties of a nanoparticle's layer. By studying experimental data received by

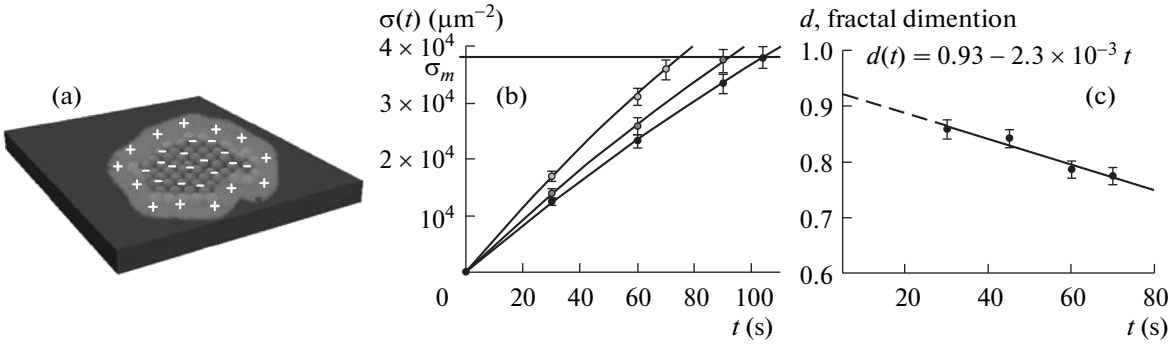

Fig. 3. Qualitative and quantitative descriptions. (a) – Qualitative model of surface polarization process. (b) – Experimental data (dots) and theoretical kinetic behavior of deposition processes with Langmuir kinetic (line) are shown. (c) – Evolution of monolayer's fractal dimension during deposition and layer growth. On this image bars show error 5% related to specific of AFM measurements

the AFM technique, we were able to define the fractal dimension of monolayers and its dependence on deposition time (see Fig. 3c). It should be noted that $N_{\max}$, obtained during the fitting of experimental data, had been close or equal to the number of particles covered by the area S_m.

The next features revealed during the deposition should be noted:

1) the second layer is not formed during the growth period of the first one;

2) the area occupied by isolated or small groups of nanoparticles on free (not occupied by a monolayer) substrate surfaces is much smaller than the area of the monolayer site.

The fact that a second layer is not formed during a whole deposition time could be explained by presence of a charge of nanopartices already attached to the surface.

According to these features the main question is why we have not observed uniform distribution of the particles along the HOPG surface. The relation between the number of particles in the monolayer (with respect to packaging density) and the number attached to the HOPG surface and free from the monolayer is about 10^2 (these calculations were done for the concentration range mentioned above). This value decreases with increasing concentration. Such behavior can be conditioned by polarization and Coulomb's interaction. The hydrophobic HOPG surface should have a negative potential energy of interaction with hydrophilic nanoparticles [17] having a charge distributed on the particle surface, while the counterions in the liquid create a coat near the surface of the particles. Being attached through the dipole-dipole interaction onto the HOPG surface nanoparticles are able to move along the atomically smooth surface. This movement can be continued till the some distance from another particle or defect on the surface. This could be the reason for the poor occupation of free surface observed during experiments on the HOPG.

Nevertheless, over time, at a certain concentration, there are particles that will overcome repulsion and attach to the surface due to the polarization of the surface and Coulomb's interaction. Having attached, the particle polarizes the surface in immediate proximity around itself and level short-range Van-der-Waals repulsion. The induced charge creates "separate" parts of the surface located on the perimeter of the monolayer which are probably energetically more favorable for adsorption of new particles from a solution (see Fig. 3a). In this case we should see a different behavior of deposition during experiments with non conductive substrates. This assumption was confirmed by our experiments with silicon oxide and glass where we observed a much lower rate of the adsorption and 3D structures formation (Fig. 4a). Formation of large clusters, we believe, was due to the fact that a lower adsorption rate led to an increase of the concentrations of nonvolatile components and a change of pH within the solution. The pH of a solution, as it is known, plays an important role in forming and maintaining the charge of nanoparticles [18, 27]. The pH change adjusts the charge of the nanoparticles which results in clusterzation [28]. It is necessary to notice that experiments with lower and higher concentrations of nanoparticles in a solution at sedimentation on HOPG also lead to growth of three-dimensional structures on a substrate. For an understanding of the low adsorption rate, we should take into account another significant difference between the HOPG and the mentioned substrates – thermal conductivity which is $\sim 2000\,\mathrm{W}\cdot\mathrm{K}^{-1}\cdot\mathrm{m}^{-1}$ for HOPG, $\sim 1.4\,\mathrm{W}\cdot\mathrm{K}^{-1}\cdot\mathrm{m}^{-1}$ for silicon oxide [29] and ~ 0.3–$10\,\mathrm{W}\cdot\mathrm{K}^{-1}\cdot\mathrm{m}^{-1}$ for glass [30]. Differences in the thermal conductivity of the water-ammonia solution $\sim 0.6\,\mathrm{W}\cdot\mathrm{K}^{-1}\cdot\mathrm{m}^{-1}$ [31] and

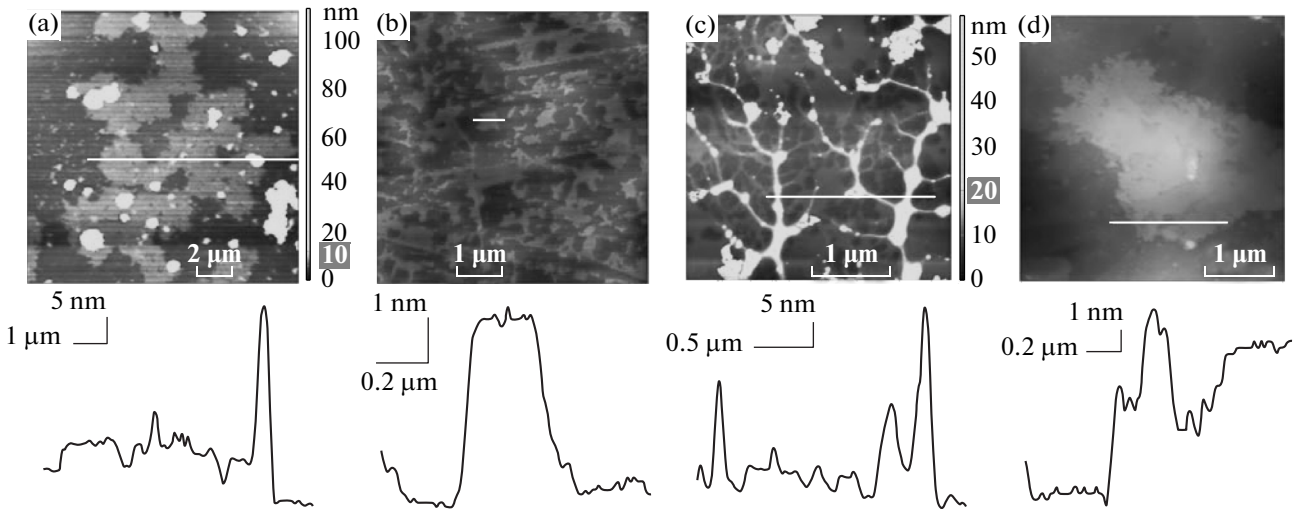

Fig. 4. Various conditions of a deposition process. The top figures are 2D AFM images obtained by tapping mode. The bottom figures are the cross-sections of the surfaces area shown on the top images by line. For all cases concentration was $C = 1.89 \cdot 10^3\ \mu\text{m}^{-3}$. Results of nanoparticles' deposition: (a) – on the glass during 120 s; (b) – on the amorphous carbon (located on the TEM grid) during 90 s; (c) – 3D structures as a result of ammonia concentration expansion. Deposition provided on the HOPG surface during 10 s. (d) – CdTe nanoparticles' multilayer after 30 s of deposition in the solution with pH = 7

HOPG could lead to the presence of flows caused by Marangoni forces and directed (in this case) from the edge of the droplet to the center and then up to the droplet-air interface. On the other hand, not pinned droplet edge and the particularly low volatility of water and consequently insignificant small difference of temperatures between water-air and the water – HOPG interface, are able to level the given effect. To ascertain influence of these flows on the adsorption kinetic, we performed experiments with an electrical conductive substrate having a low thermal conductivity coefficient – amorphous carbon ($0.6–10\ \text{W} \cdot \text{K}^{-1} \cdot \text{m}^{-1}$) [32]. These experiments have shown the same results as have been obtained for glass and silicon oxide supports (Fig. 4b).

Thus, we believe that the thermal and electrical conductivities play a key role in adsorption behavior.

In this case, using the framework of the Langmuir isotherm (1) does not give a good physical sense of the constant k_c. For the processes of classical monomolecular adsorption of a gas on a solid surface k_c should be proportional to the number of collisions of particles with a surface and to the fraction of particles able to be adsorbed onto the surface [33]. The calculated effective rate constant is equal to an increase of adsorption rate relative to an increase of the area of a monolayer and should be proportional to the fraction of particles adsorbed at collision and the number of collisions of particles on the substrate surface. If we say that the number of particles colliding with a substrate $n_{s\delta}$ is equal to the sum of the number of particles delivered to a surface at the expense of Marangoni flows N_m with the number of particles available in the near-surface layer δ and those reaching the surface in this period during Brownian motion n_δ, the effective rate constant will be:

$$k_c = \alpha n_{s\delta} = \alpha(n_\delta - N_m),$$

where α is probability of a particle attaching due to a collision. This equation doesn't let us make reasonable conclusions about the existence of Marngoni flows since we don't know value of α. We believe α is different for attaching onto the free HOPG surface and the monolayer's perimeter.

Experiments have shown that the kinetic also depends on various solution parameters: pH, solution volatility, ammonia, KOH and 3-mercaptopropionic acid (MPA) concentrations. Outside of the pH range between 8 and 9 as used in our experiments, however, the kinetic of adsorption shows drastically different behavior. For example, at a pH value of around 7 a second layer begins to form while the first layer does not fully cover the surface (see Fig. 4d). In the case of ammonia concentration expansion, the volatility of the solution increases and pH changes that result in the presence of sediment visible to the naked eye after 10 seconds of deposition take place (see Fig. 4c).

Conclusion. We have demonstrated, for the first time that CdTe nanoparticles monolayer of area about $10^4\ \mu\text{m}^2$ can be formed in less than 90 s. Our approach

may be useful in creating a homogeneous distribution of nanoparticles on a conductive surface with strong hydrophobic properties that could be applied in LED, solar cells technologies among others. This technique could be generalized to other conductive supports. The analysis of adsorption kinetics of particles on a surface shows that it is well described by the Langmuir isotherm. Experimental results found influence of the Marangoni flows caused by a difference of thermal conductivities of a solution and a substrate. Weak adsorption rate on the amorphous carbon and other low thermal conductive materials doesn't let us provide TEM measurements and make conclusions about the order of the monolayers. Answering the questions related to the qualitative description of Marangoni flows' influence and order of the self-assembled monolayer are the future directions of our work.

This research was funded by the Russian Foundation of Basic Researches (RFBR, grant #10-03-00679 to V.F.R., D.N.V., L.M.N, D.Yu.N.) and the Program of RAS Presidium (#24 "Fundamentals of Technology of Nanostructures and Nanomaterials" to V.F.R., D.N.V., L.M.N, D.Yu.N.). D.N.V. thanks Prof. A.P.Sokolov for a Postdoctoral Fellowship. The authors would like to thank S.B.Brichkin, M.G.Spirin, S.A.Kurochkin, A.N.Pyrkov, Prof. P.C.Morais, L.Yu.Barash, Prof. L.N.Shcur for their assistance and discussions.

1. A. N. Shipway, E. Katz, and I. Willner, Chem. Phys. Chem. **1**, 18 (2000).
2. C. T. Black, C. B. Murray, R. L. Sandstrom, and S. Sun, Science **290**, 1131 (2000).
3. S. A. Majetich, T. Wen, and R. A. Booth, ACS Nano **5**, 6081 (2011).
4. Z. Nie, A. Petukhova, and E. Kumacheva, Nature Nanotech. **5**, 15 (2010).
5. V. F. Puntes, P. Gorostiza, D. M. Aruguete et al., Nat. Mater. **3**, 263 (2004).
6. T. P. Bigioni, X.-M. Lin, T. T. Nguyen et al., Nature Mater. **5**, 265 (2006).
7. J. J. Urban, D. V. Talapin, E. V. Shevchenko et al., Nature Mater. **6**, 115 (2007).
8. R. D. Deegan, O. Bakajin, T. F. Dupont et al., Nature **389**, 827 (1997).
9. S. Maenosono, C. D. Dushkin, S. Saita, and Y. Yamaguchi, Langmuir **15**, 957 (1999).
10. B. A. Korgel and D. Fitzmaurice, Phys. Rev. Lett. **80**(16), 3531 (1998).
11. G. Ge and L. Brus, J. Phys. Chem. B **104**(41), 9573 (2000).
12. Z. L. Wang, Adv. Mater. **10**(1), 13 (1998).
13. X. M. Lin, H. M. Jaeger, C. M. Sorensen, and K. J. Klabunde, J. Phys. Chem. B **105**, 3353 (2001).
14. E. Rabani, D. R. Reichman, P. L. Geissler, and L. E. Brus, Nature **426**, 271 (2003).
15. L. Yu. Barash, T. P. Bigioni, V. M. Vinokur, and L. N. Phys. Rev. E **79**, 046301 (2009).
16. L. E. Scriven and C. V. Sternling, Nature **187**, 186 (1960).
17. M. P. Pileni, J. Phys. Chem. B **105**, 3358 (2001).
18. A. Kampes and B. Tieke, Materials Science and Engineering C **8–9**, 195 (1999).
19. A. Snezhko and I. S. Aranson, Nature Materials **10**, 698 (2011).
20. P. Rodgers, Nature Nanotechnology **2**, 342 (2007).
21. Z. Tang, N. A. Kotov, and M. Giersig, Science **297**, 237 (2002).
22. M. Grzelczak, J. Vermant, E. M. Furst, and L. M. Liz-Marzán, ACS Nano **4**(7), 3591 (2010).
23. W. W. Yu, Y. A. Wang, and X. Peng, Chem. Mater. **15**, 4300 (2003).
24. S. F. Wuister, I. Swart, F. Van Driel et al., Nano Lett. **3**(4), 503 (2003).
25. M. J. Frank, J. A. M. Kuipers, and W. P. M. van Swaaij, J. Chem. Eng. Data **41**, 297 (1996).
26. D. A. Frank-Kamenetskii, *Diffusion and Heat Transfer in Chemical Kinetics*, Plenum Press, N.Y., 1969.
27. F. Qu and P. C. Morais, J. Phys. Chem. B **104**(22), 5232 (2000).
28. J. Richardi, J. Chem. Phys. **130**, 044701 (2009).
29. S. M. Sze, *Physics of Semiconductor Devices*, John Wiley and Sons, Inc., N.Y., 1981.
30. L. C. Hulstrom, *Thermal Conductivity Ch.19*, Plenum Press, N.Y., 1988.
31. D. P. Needham and H. Ziebland, Int. J. of Heat and Mass Trans. **8**(11), 1387 (1965).
32. S. R. P. Silva, *Properties of Amorphous Carbon*, INSPEC, London, 2003.
33. D. K. Schwartz, Annu. Rev. Phys. Chem. **52**, 107 (2001).